Available online at www.sciencedirect.com
SCIENCE DIRECT®
Journal of Solid State Chemistry 177 (2004) 1803–1810
JOURNAL OF SOLID STATE CHEMISTRY
http://elsevier.com/locate/jssc

Evolution of structural features and mechanical properties during the conversion of poly[(methylamino)borazine] fibers into boron nitride fibers

Samuel Bernard,* Khaled Ayadi, Marie-Paule Berthet, Fernand Chassagneux, David Cornu, Jean-Marie Letoffe, and Philippe Miele*

Laboratoire des Multimatériaux et Interfaces, UMR CNRS 5615, Université Claude Bernard-Lyon 1, 43, Bd du 11 Novembre 1918, 69622 Villeurbanne Cedex, France

Received 15 October 2003; received in revised form 9 January 2004; accepted 14 January 2004

Abstract

Poly[(methylamino)borazine] (PolyMAB) green fibers of a mean diameter of 15 μm have been pyrolyzed under ammonia up to 1000°C and heat treated under nitrogen up to 2000°C to prepare boron nitride (BN) fibers. During the polymer-to-ceramic conversion, the mechanical properties of the green fibers increase within the 25–400°C temperature range owing to the formation of a preceramic material and remain almost constant up to 1000°C. Both the crystallinity and the mechanical properties slightly increase within the 1000–1400°C range, in association with the consolidation of the fused-B_3N_3 basal planes. A rapid increase in tensile strength (σ^R) and elastic modulus (Young's modulus E) is observed in relation with crystallization of the BN phase for fibers treated between 1400°C and 1800°C. At 2000°C, "meso-hexagonal" BN fibers of 7.5 μm in diameter are finally obtained, displaying values of $\sigma^R = 1.480$ GPa and $E = 365$ GPa. The obtention of both high mechanical properties and fine diameter for the as-prepared BN fibers is a consequence of the stretching of the green fibers on a spool which is used during their conversion into ceramic.
© 2004 Elsevier Inc. All rights reserved.

Keywords: Boron nitride; Ceramic fiber; Preceramic polymer; Polymer-to-ceramic conversion; Ceramization; Crystallization

1. Introduction

Although the ability of specific polymers to be converted into covalently bonded ceramics (polymer-derived ceramics, PDCs) is known for a long time [1], much attention has been focused recently on the preceramic polymer route for the production of shape-controlled ceramics [2–6]. One significant advantage of this method is that ceramic fibers with fine diameters can be elaborated from tractable polymers after spinning and pyrolysis steps [4,7]. Thus, following the approaches of Winter et al. [8] and Yajima et al. [9] on fibers around Si-based systems (SiC and SiC/Si_3N_4 fibers), considerable interest has been dedicated to the preparation of melt-processible preceramic polymers and their conversion into various non-oxide ceramic fibers. These polymers are usually composed of an inorganic backbone bearing organic groups whose nature determines to a certain extent the polymer processability [10,11]. These pendent groups are partly released during the pyrolysis process to yield an amorphous and covalent ceramic at moderate temperature. Depending on the application, a subsequent optional high temperature heat treatment allows this preceramic material to be transformed into a stable crystalline ceramic [12–15]. As illustrations of this method, one could refer to the preparation of carbon fibers and silicon carbide fibers from polyacrilonitrile [16] and polycarbosilane [17,18], respectively.

Many boron and nitrogen containing polymers have been described in the literature [19–24]. They have been synthesized for various applications in several forms such as boron nitride (BN)-based bulk materials, matrices, thin films and coatings [25–30]. In the case of BN fibers, poly[(alkylamino)borazines] have proven to be the most attractive precursors [31–34]. Kimura et al. have prepared a condensat from a mixture of

*Corresponding authors. Fax: +33-4-72-44-06-18.
E-mail addresses: samuel.bernard@univ-lyon1.fr (S. Bernard), philippe.miele@univ-lyon1.fr (P. Miele).

0022-4596/$ - see front matter © 2004 Elsevier Inc. All rights reserved.
doi:10.1016/j.jssc.2004.01.004

B-tri(methylamino)borazine (MAB) and laurylamine [31]. This condensat is tailored to be meltable and spinnable. Resulting BN fibers elaborated at high temperature (1800°C) exhibited good mechanical properties ($\sigma^R = 1000$ MPa, $E = 80$ GPa) and fine diameters ($\phi \sim 10\,\mu m$). Following this approach, BN fibers were obtained from alkylaminoborazine-derived polymers [32] and particularly poly[2,4,6-tri(methylamino)borazine] (polyMAB) [33]. This type of polymer can present rheology, reactivity and thermal properties suitable for the preparation of BN fibers with fine diameter and high mechanical properties by spinning and pyrolysis processes. After the melt-spinning of the polyMAB, the pyrolysis of the resulting green fibers was performed in two steps: (1) under ammonia up to 1000°C and (2) under nitrogen up to 2000°C. In a preliminary study, we described the chemical modifications involved during the polymer-to-ceramic conversion [34]. In the present work, this preliminary study has been completed by studying, during the entire conversion process, the evolution of the structural features of the fibers (crystallite sizes, crystallization degree, etc.) and their physical properties including density, diameter and mechanical properties (tensile strength σ^R and Young's modulus E).

2. Experimental

2.1. Preparation of BN fibers

All reactions yielding to the preceramic polymer were carried out in a purified argon atmosphere using standard Schlenk techniques. The starting monomer, 2,4,6-tri(methylamino)borazine (MAB), has been synthesized following a procedure described in the literature [35]. The poly[(alkylamino)borazine] (polyMAB) has been prepared by a bulk thermolysis of MAB under argon. The monomeric units polymerize with the gradual increase of the temperature up to 200°C to form a soluble and meltable solid.

Polymeric green fibers were produced in nitrogen atmosphere using a lab-scale spinning apparatus set up in a glove-box. The polyMAB was then softened by heating into a heater block up to 180°C and forced by a piston through the heater block and finally through a mono-hole spinneret with a 0.2 mm capillary. The molten polymer emerging from the capillary as an endless fiber was stretched by a rotating spool with a drawdown ratio of 13.3 (diameter of the polyMAB fiber emerging from the capillary (before stretching)/diameter of the polyMAB fiber after stretching) into a continuous fiber having a diameter of $\sim 15\,\mu m$. The green fiber collected on the take-up spool was converted into a ceramic fiber by a two-step pyrolysis process. The green fiber was first subjected to a heat treatment under ammonia from 25°C to 1000°C in order to remove the carbon contaminants [34] then to a further heat treatment at high temperature up to 2000°C under nitrogen atmosphere to ensure its complete conversion into a BN fiber. The fiber wound on the spool was pyrolyzed at 0.8°C min^{-1} and kept 10 min at different final temperatures from 100°C to 2000°C before quenching. At the end of the process, the wound continuous BN fiber was cut along the spool into short bundles. The detailed physical and chemical data for polymer, pyrolyzed fibers and ceramic fibers are listed in Table 1.

Table 1
Physical and chemical data for polymer, pyrolyzed fibers and ceramic fibers

Glass temperature of the polyMAB	90°C
Spinning temperature of the polyMAB	180°C
Empirical formula of the polyMAB[a]	$C_{0.7}N_{1.5}BH_{3.1}$
Empirical formula of the fibers pyrolyzed at 200°C[a]	$C_{0.4}N_{1.4}BH_{2.5}$
Empirical formula of the fibers pyrolyzed at 400°C[a]	$C_{0.3}N_{1.4}BH_{2.4}$
Empirical formula of the fibers pyrolyzed at 800°C[a]	$C_{0.1}N_{1.1}BH_{0.9}$
Empirical formula of the fibers pyrolyzed at 1000°C[a]	$N_{1.1}BH_{0.7}$
Empirical formula of the fibers pyrolyzed at 1500°C[a]	$N_{0.92}B$

[a] Oxygen values were determined to be lower than 2 wt%.

2.2. Characterization

As the polymer and resulting fibers pyrolyzed up to 1400°C are reactive towards moisture and oxygen, the following sample preparations were performed within a glove box in an argon environment. Differential scanning calorimetry (DSC) analyses (Mettler Toledo DSC TA 8000) were performed under argon between −10°C and 170°C using a heating rate of 10°C min^{-1} from ~15.0 mg of polymer placed in an aluminum crucible. Elemental analysis were performed by Le Service Central de Microanalyze du CNRS (Vernaison, France) on the polyMAB and fibers pyrolyzed at 200°C, 400°C, 800°C, 1000°C and 1500°C.

X-ray diffraction (XRD) analysis (Phillips PW 1830/40) with a Cu$K\alpha$ radiation source was carried out at room temperature according to two procedures. At first, the $\theta - 2\theta$ XRD patterns were recorded in the range 20°–60° from a bundle, i.e., the fibers in the bundle were perpendicularly oriented to the $\theta - 2\theta$ plane. Subsequently, the XRD patterns were recorded in the range 20°–90° from the same fibers but after grinding. Both types of XRD analysis give sufficient information to allow a complete structure and texture analysis from the following parameters:

(a) the interlayer spacing d_{002};
(b) the average height $\bar{L}_{c(002)}$ of the stacks of layers;
(c) the average length $\bar{L}_{a(10)}$ of the BN layers;
(d) the degree of crystallization η;

(e) the degree of orientation ω of the hexagonal layers compared to the fiber axis.

$d_{0\,0\,2}$ was calculated from Bragg equation using the diffraction angle of the (002) peak while the average stack height $\bar{L}_{c(002)}$ and length $\bar{L}_{a(10)}$ values were calculated from the Scherrer equations:

$$\bar{L}_{c(002)} = 0.9\lambda/(B^2 - B'^2)^{1/2}\cos\theta, \quad (1)$$

$$\bar{L}_{a(10)} = 1.84\lambda/(B^2 - B'^2)^{1/2}\cos\theta, \quad (2)$$

where λ is the Cu$K\alpha_1$ wavelength ($\lambda = 0{\cdot}154$ nm), θ the Bragg angle of the (002) and (10) diffraction peaks, respectively, B the full-width at half-maximum intensity (FWHM) of the corresponding peaks and B' the instrumental contribution.

The structural parameters $\bar{L}_{c(002)}$ and $\bar{L}_{a(10)}$ represent the apparent average dimensions of the coherent crystalline domains parallel and perpendicular to the crystallite c-axis, respectively. The word "apparent" emphasizes that the diffraction line shapes depend also on the crystal structure imperfections. However, discrepencies related to the interpretation of $\bar{L}_{c(002)}$ and $\bar{L}_{a(10)}$ parameters still remain. It has been established through transmission electron microscopy studies of high-performance BN fibers [33] that the length of the continuous BN layers and the height of the BN stacks were very much greater than $\bar{L}_{c(002)}$ and $\bar{L}_{a(10)}$ as determined by XRD, respectively, since the BN layers are actually bended and twisted. [33] Hence, $\bar{L}_{c(002)}$ and $\bar{L}_{a(10)}$ may be better interpreted as the average dimension of the "straight parts" of the BN stacks. Moreover, the XRD pattern may also depend on the orientation of the analyzed materials, especially for textured solids elaborated at high temperature. Indeed, analyses performed on fibers pyrolyzed above 1400°C revealed a preferential orientation of the layers along the fiber, as evidenced by the increase of the intensity of (002) peak relatively to that of the (10) peaks. The estimation of $\bar{L}_{a(10)}$ may therefore be inexact because of the very low intensity of the (10) peak and furthermore some diffraction peaks may be missing especially above $2\theta = 60°$. To avoid that, the XRD patterns were recorded from the same fibers but after grinding. In this case, the hexagonal layers are randomly oriented in the material.

The calculation of the relative degree of crystallization η was proposed by Toy et al. [37] from the half intensity values of the (002) diffraction peaks in X-ray diffractograms. An increase in the intensity of the (002) peak involves the increase of η from 0 to 1. The half intensity of the highest (002) peak of the polyMAB-derived fiber pyrolyzed at 2000°C corresponds to $\eta = 1$. The preferred orientation degree ω of the hexagonal layers in a direction parallel to the fiber axis was obtained by comparing the intensity ratio of the (002) and (10) peaks in both XRD patterns obtained from bundles and ground-up samples.

$$\omega = (R_{\text{fibers}} - R_{\text{ground up fibers}})/R_{\text{fibers}}, \quad (3)$$

where R is the ratio between the (002) and (10) peak intensities in the diffractogram: $R = I_{(002)}/I_{(10)}$.

The density measurements were carried out with a helium pycnometer. The tests were realized from 1 g of samples of green and pyrolyzed fibers (200°C, 500°C, 1100°C, 1500°C, 1800°C and 2000°C).

Tensile tests at room temperature and diameter measurements were performed from single fibers with a gauge length of 10 mm. 50 individual fibers were taken from several final bundles throughout to incorporate any possible property variation within the lot in fiber fracture statistics and both ends of each fiber were glued with cyanocrylate on a cardboard before handling and testing. Their diameter was measured by laser interferometry and an average diameter was determined. Tensile tests were achieved from a standard tensile tester (Adamel Lhomargy DY 22) equipped with two grips, a displacement transducer and a load cell (5 N). The crosshead speed was 0.1 mm/min. Achieving good alignment of fibers with the grips and load axis was critical to obtain accurate load values. Fiber strain ε (%) and Young's modulus E (GPa) were measured for each fiber from data of the load–elongation curves (elongation of fibers and breaking load) and diameters. Values of fiber strain and Young's modulus were then corrected with a corrective factor taking into account the deformation of grips during the mechanical traction of each fiber. The strain and Young's modulus were evaluated by averaging the results of the 50 mechanical tests. The failure strength values are lightly scattered due to the presence of flaws along fibers. A statistical Weibull distribution was used to describe the failure strength σ^R data [38]. In accordance with Weibull model, each increasing value of tensile strength was associated with a probability of failure P giving by Eqs. (4) and (5):

$$P = (i - 0.3)/(n - 0.4), \quad (4)$$

$$P = 1 - \exp[-(V/V_0)(\sigma/\sigma_0)^m], \quad (5)$$

where i represents the rank of strength, n the overall number of mechanical tests ($n = 42$), V the tested volume, σ the strength and m the Weibull modulus. V_0 and σ_0 are the scaling constants. m estimates the dispersion of strength values. The lower the value of m, the greater the dispersion of strength.

By rearranging and taking the natural logarithm of both sides of the Eq. (2), the following Eq. (6) was obtained:

$$\text{Ln}[\ln(1/(1-P))] - \ln(V/V_0) = 1 + m\ln\sigma - m\ln\sigma_0, \quad (6)$$

The final strength of the BN fibers was estimated for a failure probability of 0.632.

3. Results and discussion

3.1. XRD and density measurements of polyMAB-derived fibers as a function of the pyrolysis temperature

During the transformation of polyMAB to BN fibers up to 2000°C, the XRD features (Figs. 1 and 2) change from diffuse (002) and (10) diffraction lines characteristic of an amorphous material (PolyMAB fibers) to the well-defined peaks of a well-obvious crystalline ceramic (PolyMAB fibers pyrolyzed at $T = 1800$°C and 2000°C).

Due to these changes in XRD patterns, the textural and structural parameters vary with the heat treatment temperature. For instance, the variation of $\bar{L}_{c(002)}$ and $\bar{L}_{a(10)}$ as well as the interlayer $d_{0\,0\,2}$ spacing of the fibers during their polymer-to-ceramic conversion is shown in Fig. 3.

In the range 20–1000°C (crosslinking and mineralization steps), there is no major modification in both XRD patterns and the crystalline structure of the fibers. The diffuse diffraction peaks remain asymmetric, broad and the 2θ positions are distant from those in h-BN crystal [36]. Even if it is difficult to determine the grain size for fibers pyrolyzed below 1000°C due to the broad peaks, the apparent average grain size ($\bar{L}_{c(002)}$ and $\bar{L}_{a(10)}$) remains almost unchanged and the value of the interlayer d-spacing $d_{0\,0\,2}$ reaches rapidly a plateau indicating a high amount of disorder in the structure of the fibers, which can be correlated with the low relative degree of crystallization η in this range. However, the monitoring of the different parameters clearly show that the crystallization process begins at 1000°C. A slight increase in the intensities of the (00l) reflections is evidenced. The value of η starts to increase slowly from 1000°C and more quickly from 1300°C (Fig. 4). In the range 1000–1400°C (ceramization step), the apparent average grain size increases slightly but remains smaller than about 1.4 and 5.1 nm for $\bar{L}_{c(002)}$ and $\bar{L}_{a(10)}$, respectively, which is relatively close to the values measured at 1000°C. Although the crystallization state in the fibers elaborated at 1400°C is slightly

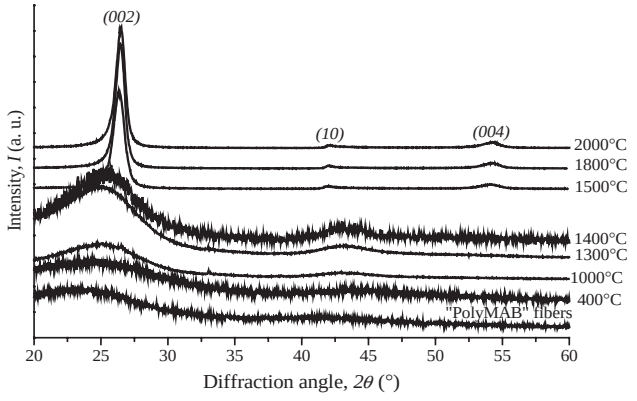

Fig. 1. XRD patterns of the polyMAB-derived fibers as a function of the pyrolysis temperature.

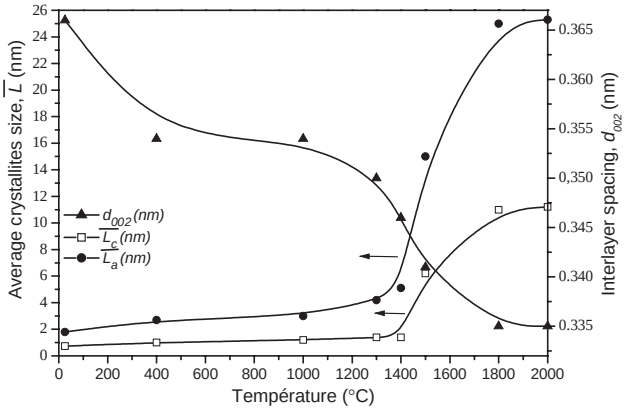

Fig. 3. Changes in $\bar{L}_{c(002)}$, $\bar{L}_{a(10)}$, and $d_{0\,0\,2}$ as a function of the pyrolysis temperature.

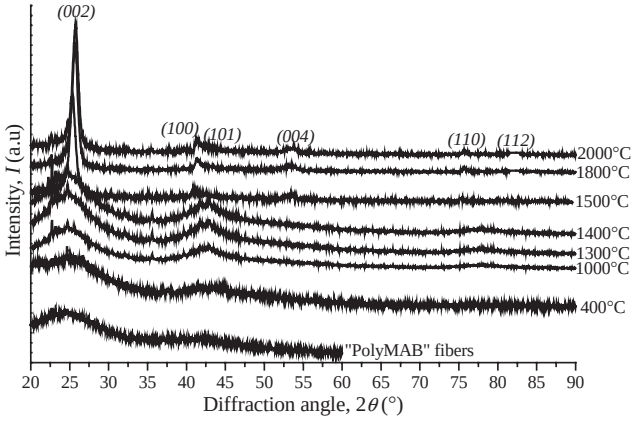

Fig. 2. XRD patterns of the ground-up samples of the polyMAB-derived fibers as a function of the pyrolysis temperature.

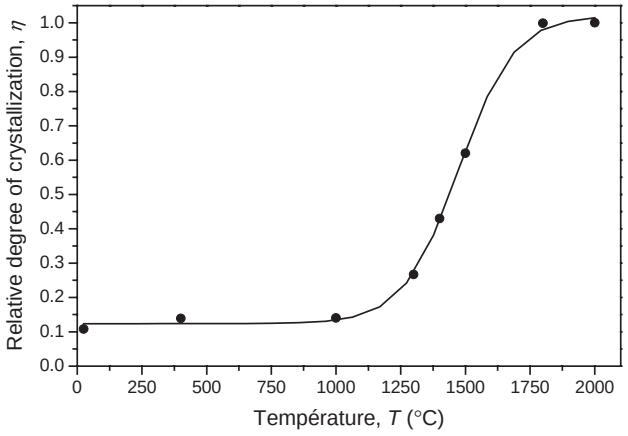

Fig. 4. Changes in η as a function of the pyrolysis temperature.

Table 2
Degree of orientation of the crystallites along the fiber axis estimated from the relative intensity of (002) ($I_{(002)}$) and (10) peaks ($I_{(10)}$) in both type of XRD patterns

Heat treatment temperature (°C)	1400	1500	1800	2000
$I_{(002)}$ (%) in Figs. 1 and 2	100	100	100	100
$I_{(10)}$ (%) in Fig. 1	16.2	2.3	1.2	1.3
$I_{(10)}$ (%)in Fig. 2	41	7.8	7.4	7.4
Degree of orientation of the crystallite ω	0.60	0.71	0.84	0.84

improved compared to that of the fibers pyrolyzed at 1000°C, the BN phase remains poorly ordered as confirmed by the low value of η ($\eta = 0,40$) and by the value of $d_{0\,0\,2}$ ($d_{002} = 0.346$ nm), higher than that in a h-BN (0.3327 nm) [36].

Likewise, Table 2 showing the degree of orientation of the crystallites along the fiber axis ($0 \leqslant \omega \leqslant 1$, see Section 2) as a function of the pyrolysis temperature in the range 1400–2000°C indicates that the (002) layer misalignement is relatively large up to 1400°C.

The XRD patterns are brutally modified above 1400°C which indicates a strong variation of the textural and structural parameters, especially in the temperature range 1400–1500°C. The 2θ values for each diffraction peak become closer to the h-BN theoretical data [36] and the intensity of the (002), (004), (110) and (112) lines increases with the pyrolysis temperature which means an ordering of the structure.

At 1500°C, the average grain size is around 6.2 and 15 nm for $\bar{L}_{c(002)}$ and $\bar{L}_{a(10)}$, respectively, and the interlayer $d_{0\,0\,2}$ spacing is 0.341 nm. The crystallization of the BN phase also improves as shown by the increase of η to about 0.65. The degree of orientation of the crystallites along the fiber-axis also increases ($\omega = 0.71$) (Table 2). Although the BN layers tend to stack parallel to each other at 1500°C, the $d_{0\,0\,2}$ value is characteristic of a turbostratic phase. Above 1500°C, the modifications in the XRD patterns are minor. The samples annealed at 1800°C and 2000°C show the sharp (002) peaks with a higher intensity and the (10) and (004) reflections corresponding, respectively, to d spacings of $\sim$0.335 nm ($2\theta_{(002)} = 26.57°$), $\sim$0.215 nm ($2\theta_{(10)} = 41.97°$) and $\sim$0.169 nm ($2\theta_{(004)} = 54.20°$). The average grain size increases from 6.20 and 15.0 nm (1500°C) to 10 and 32 nm (1800°C), for $\bar{L}_{c(002)}$ and $\bar{L}_{c(002)}$, respectively (Fig. 3). The relative degree of crystallizations becomes maximal ($\eta = 1$) at 1800°C suggesting that the crystallization process is achieved at this temperature. The degree of crystallites orientation also reaches its maximal value ($\omega = 0.84$) at 1800°C. Nevertheless, the difference observed in the in-plane lattice parameter as compared to the h-BN values [36] reveals the presence of imperfectly ordered layers in the samples. This is confirmed by the lack of (102) type of reflections ($2\theta_{(1\,0\,2)} = 50.15°$ [36]) in all diffraction patterns (Fig. 2). However, local hexagonal domains exist in the fibers elaborated from 1800°C as indicated by the presence, in the XRD patterns of ground-up fibers, of the low intensity (110) and (112) lines as well as the (10) peak which tends to resolve into the (100) and (101) lines. Therefore the structure is only partially three-dimensionally ordered as suggested by Hubacek et al. [39] and Thomas et al. [40]. The BN phase in the fibers obtained in the range 1800–2000°C can be described as a "meso-hexagonal" structure, which corresponds to a transitional phase between turbostratic and hexagonal structure. The X-ray studies show that the large crystallites (Fig. 3) are arranged around the longitudinal axis of the fiber with their basal planes highly oriented parallel to the axis ($\omega = 0.84$, Table 2) in the BN fibers elaborated at 1800°C and 2000°C.

A relevant aspect in polyMAB fibers pyrolysis is the change in density and volume during the heat treatment. The evolution of the density of the polyMAB-derived fibers measured during the whole process is reported in Fig. 5 and the continuous variation can be correlated with the changes in the XRD data. While the density of green fibers is typically 1.20, a significant densification is observed within the range 20–400°C, which can be related to the condensation and the branching of the macromolecules (crosslinking step) associated with the release of methylamine during the first step of the conversion under ammonia atmosphere. The increase of density is well-associated with the decrease of the d-spacing $d_{0\,0\,2}$ (Fig. 3).

The density moderately increases (at 1000°C, $d = 1.55$ and 1400°C, $d = 1.66$), in accordance with the progress in the crosslinked polymer-to-ceramic transformation and the slow improvement of η. Finally, the rapid increase of the density within the range 1400–2000°C (from $d = 1.66$ to 1.95) corresponds to the crystallization process. It is specially associated with the marked decrease of $d_{0\,0\,2}$ (Fig. 3). The final density is nevertheless lower than the theoretical value for h-BN

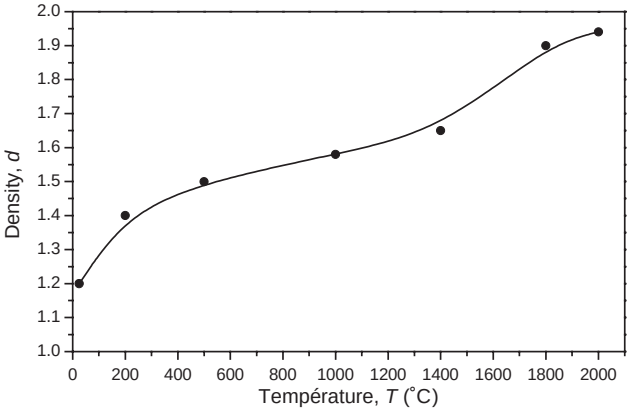

Fig. 5. Changes in the density of the polyMAB-derived fibers as a function of the pyrolysis temperature.

($d = 2.27$). The low value of density (1.95) obtained at 2000°C can be explained by the high porosity degree (value of 14%) in the BN fibers as previously observed [33].

3.2. Changes in the tensile strength and Young's modulus of polyMAB-derived fibers as a function of heat treatment temperature

Five uniaxial load/strain curves obtained at room temperature from polyMAB-derived fibers pyrolyzed up to 400°C, 1000°C, 1400°C, 1500°C or 1800°C are shown in Fig. 6. Each fiber shows a brittle character.

The handle and flexible fibers pyrolyzed below 1400°C show relative high strain but they could not be used as reinforcement agent at this temperature because they support only a low tensile load. Between 1400°C and 1500°C, the applied load has to increase in order to break the fibers and above 1500°C, the failure strain and the stiffness increase owing to the crystallization step identified from 1400°C to 1800°C. The influence of the final pyrolysis temperature on the mechanical properties (σ^R, E) of the polyMAB-derived fibers deduced from data reported in Fig. 6 is evidenced in Fig. 7.

The mechanical properties of the polyMAB fibers could not be estimated due to their high brittleness and their air-sensitivity. Fig. 7 shows a simultaneous increase of the tensile strength σ^R and the Young's modulus E according to two steps up to 2000°C. First, the tensile strength and the Young's modulus both slightly increase between 100°C and 400°C up to $\sigma^R = 0.240$ GPa and $E = 17$ GPa, respectively. In this temperature range, the crosslinking process is associated with the formation of further strong covalent bonds within the structure of the preceramic network.

As already observed for the variation of the structural parameters (Figs. 3 and 4) and the density (Fig. 5), the tensile strength and the Young's modulus slowly

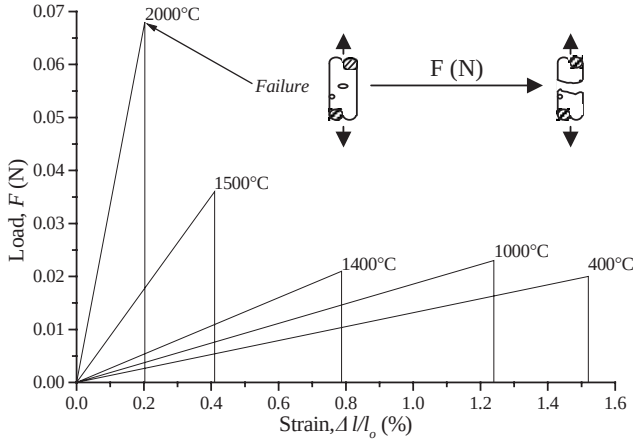

Fig. 6. Load–displacement curves of the polyMAB-derived fibers as a function of the pyrolysis temperature.

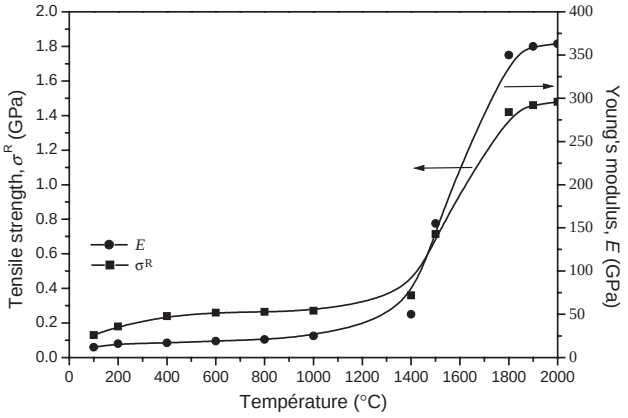

Fig. 7. Changes in the tensile strength and the Young's modulus of the polyMAB-derived fibers as a function of the pyrolysis temperature.

increase in the range 400–1000°C (mineralization process), certainly due to transamination reactions generating numerous structural rearrangements in the basal preceramic network. The values of mechanical properties obtained at 1000°C reach $\sigma^R = 0.270$ GPa and $E = 23$ GPa. Increasing the temperature above 1000°C produces the formation of longer and broader B_3N_3 basal planes in the mineral network through intermolecular reactions and the elimination of ammonia [34]. This conversion associated with the consolidation of the B_3N_3 rings is logically accompanied at 1400°C by a slight increase in tensile strength and Young's modulus ($\sigma^R = 0.360$ GPa and $E = 40$ GPa). These low values are consistent with the low relative degree of crystallization of the BN fibers at this temperature. Indeed, a higher temperature has to be applied to increase the mechanical properties through the crystallization of the BN phase. The tensile strength and the Young's modulus regularly increase with the pyrolysis temperature from 1400°C and an almost linear relationship between the mechanical properties and the temperature is observed in the range 1400–1800°C ($\sigma^R = 1.420$ GPa, $E = 340$ GPa). This trend can be attributed to the increase in the relative degree of crystallization, crystallite size and preferential orientation of the fused B_3N_3 structure along the fiber axis.

The mechanical properties reach high values at 1800°C and the similarities in tensile strength and modulus of the fibers pyrolyzed at 1800°C ($\sigma^R = 1.420$ GPa and $E = 340$ GPa) and 2000°C ($\sigma^R = 1.480$ GPa and $E = 365$ GPa) indicate that the structure undergoes only slight modifications within this temperature range. This is in accordance with the similar values of the d-spacing and crystallite sizes (Fig. 3), the relative degree of crystallization of the BN phase (Fig. 4), and the degree of orientation of the crystallites (Table 2) at 1800°C and 2000°C.

As it can be seen in Table 3, the Weibull modulus m (which tends to decrease with increasing dispersion

Table 3
Weibull modulus (m) and failure sections after tensile tests of the polyMAB-derived fibers as a function of the pyrolysis temperature

	Pyrolysis temperature (°C)					
	400	1000	1400	1500	1800	2000
m	5.2	5.33	5.11	3.1	2.9	3.2
Cross-section	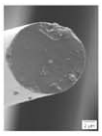	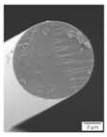	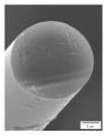	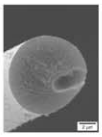		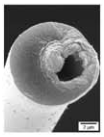

Table 4
Effect of the shrinkage of the polyMAB-derived fibers on the graphite spool

		ϕ (μm)	σ^R (GPa)	E (GPa)	ω
Pyrolysis without spool	BN fiber (1800°C)	12	0.950	60	0.60
Pyrolysis with spool	BN fiber (1800°C)	7.8	1.420	340	0.84

strength) is higher for the fibers pyrolyzed in the temperature range 400–1400°C than for the fibers pyrolyzed from 1500°C to 2000°C. Examples of SEM micrographs obtained after the mechanical tests are consistent with these results. In the range 400–1400°C, it is difficult to identify any defect in the volume of the fibers. Conversely, flaws locally appear in the failure section of some fibers pyrolyzed above 1400°C. When the fibers are pyrolyzed below 1400°C, they break due to their low intrinsic tensile strength, while above 1400°C, some fibers break due to large defects (Table 3) resulting in a decrease in the values of the Weibull modulus (i.e., in a wider dispersion of the tensile strength), without any change in the Young's modulus. The tensile strength of the fibers is not directly related to the intrinsic structure of the material but rather depends on random large defects which cause the fracture of the fibers. Further works are needed and are in progress to understand precisely the relationship between the mechanical properties and the microstructure of the BN fibers.

These high values of mechanical properties are the consequence of the longitudinal mechanical tension imposed on the fibers on the spool due to the shrinkage during sintering. As shown in Table 4, the tensile strength and the Young's modulus are significantly improved whereas the diameter reduction is higher when the fibers is stressed (Pyrolysis on a spool) than without strain (pyrolysis without spool).

The improvement in tensile strength is naturally related to the tension applied to the fibers during processing through the decrease in diameter. Restraining the longitudinal shrinkage also induces on additional crystallite orientation, further increasing mechanical properties as shown by the increase of the orientation degree of crystallites along the fiber-axis (ω, Table 4). Further works are in progress to clarify this point, quantify the maximal tension which should be imposed to the fibers and determine the essential stage(s) of the polymer–ceramic conversion during which a stress must be applied to improve the fiber mechanical properties.

4. Conclusion

The evolution of structural and mechanical properties of poly[2,4,6-tri(methylamino)borazine] fibers during their conversion into BN fibers has been studied. This work showed that the mechanical tension applied during the whole conversion process to the continuous fiber by winding on a spool improved its mechanical properties. The fiber density, Young's modulus and tensile strength increased simultaneously during the initial step of the pyrolysis 25–400°C (crosslinking step) with the formation of a basal three-dimensional preceramic network inducing an important stretching of the fiber. This led to a flexible infusible fiber with a low diameter. The structural features and mechanical properties slowly varied within the temperature range 400–1000°C (second step), corresponding to a mineralization process and leading to a slightly hydrogenated BN fiber. Its structure already showed fused B_3N_3 basal planes with an incomplete consolidation. During the mineral-to-ceramic conversion from 1000°C to 1400°C (third step), the B_3N_3 basal planes gradually consolidated but the relative degree of crystallization remained low at 1400°C. At this stage, the low mechanical properties of the BN fiber emphasized the need of a high-temperature treatment to complete its crystallization and the increase of its mechanical properties. Indeed, the mechanical properties (σ^R, E) and the size of the crystallites rapidly increased between 1400°C and 1500°C. The orientation of the hexagonal layers along the fiber axis and the structure of the BN phase were strongly improved from 1400°C to 1800°C (fourth step). A turbostratic structure was obtained at 1500°C whereas large crystallites of a

partially three-dimensional h-BN structure (meso-hexagonal) were obtained at higher temperature (1800°C and 2000°C). The *c*-axis of the crystallites was preferentially oriented normal to the fiber axis resulting in high mechanical properties.

References

[1] P.G. Chantrell, P. Popper, in: P. Popper (Ed.), Inorganic Polymers and Ceramics, Special Ceramics, Academic Press, New York, 1965, p. 87.
[2] S. Yajima, Philos. Trans. Roy. Soc. A 294 (1980) 419.
[3] R. Riedel, M. Seher, J. Mayer, D.V. Szabo, J. Eur. Ceram. Soc. 15 (1995) 703.
[4] K.J. Wynne, R.W. Rice, Ann. Rev. Mater. Sci. 14 (1984) 297.
[5] G.C. Wei, C.R. Kennedy, L.A. Harris, Am. Ceram. Soc. Bull. 63 (1984) 1054.
[6] W.R. Schmidt, V. Sukumar, W.J. Hurley Jr., R. Garcia, R.H. Doremus, L.V. Interrante, G.M. Renlund, J. Am. Ceram. Soc. 73 (1990) 2412.
[7] K. Okamura, Composites 18 (1987) 107.
[8] G. Winter, W. Verbeek, M. Mansmann, US Patent 3892583 (1975).
[9] S. Yajima, J. Hayashi, M. Omori, K. Okamura, Nature 261 (1976) 683.
[10] M. Weinmann, R. Haug, J. Bill, F. Aldinger, J. Schuhmacher, K. Müller, J. Organometal. Chem. 541 (1997) 345.
[11] E. Kroke, Y.-L. Li, C. Konetschny, E. Lecomte, C. Fasel, R. Riedel, Mater. Sci. Eng. 26 (2000) 97.
[12] Y.D. Blum, K.B. Schwartz, R.M. Laine, J. Mater. Sci. 24 (1989) 1707.
[13] P. Greil, Adv. Eng. Mater. 2 (2000) 339;
P. Greil, Adv. Mater. 14 (2002) 709.
[14] G.D. Soraru, F. Babonneau, J.D. Mackenzie, J. Mater. Sci. 25 (1990) 3886.
[15] D. Kurtenbach, H.-P. Martin, E. Müller, G. Roewer, A. Hoell, J. Eur. Ceram. Soc. 18 (1998) 1885.
[16] M.K. Jain, A.S. Abhiraman, J. Mater. Sci. 22 (1987) 278.
[17] C.L. Schilling, J.P. Wesson, T.C. Williams, J. Polym. Sci. 70 (1983) 121.
[18] T. Shimoo, I. Tsukada, M. Narisawa, T. Seguchi, K. Okamura, J. Ceram. Soc. Jpn. 105 (1997) 559.
[19] I.B. Atkinson, B.R. Currel, Inorg. Macromol. Rev. 1 (1971) 203.
[20] H. Steinberg, R.J. Brotherton, Organoboron Chemistry, Wiley, New York. 1966, p. 175.
[21] A. Finch, J.B. Leach, J.H. Morris, Organometal. Chem. Rev. 4 (1969) 1.
[22] M.F. Lappert, G.J. Leigh, Developments in Inorganic Polymer Chemistry, Elsevier, New York, 1962, p. 20.
[23] R.T. Paine, L.G. Sneddon, Chemtech 24 (1994) 29.
[24] R.T. Paine, C.K. Narula, Chem. Rev. 90 (1990) 73.
[25] D.-P. Kim, C.G. Cofer, J. Economy, J. Am. Ceram. Soc. 78 (1995) 1546.
[26] M.G.L. Mirabelli, L.G. Sneddon, J. Am. Chem. Soc. 110 (1988) 3305.
[27] W.S. Rees, D. Seyferth, J. Am. Ceram. Soc. 71 (1988) C194–C196.
[28] C.K. Narula, R.T. Paine, R. Schaeffer, Mater. Res. Soc. Symp. Proc. 73 (1986) 383.
[29] K.J.L. Paciorek, R.H. Kratzer, Eur. J. Solid State Inorg. Chem. 29 (1992) 101.
[30] V.Z.-H. Chan, J.B. Rothman, P. Palladino, L.G. Sneddon, R.J. Composto, J. Mater. Res. 11 (1996) 373.
[31] Y. Kimura, Y. Kubo, N. Hayashi, Comput. Sci. Technol. 51 (1994) 173.
[32] B. Toury, P. Miele, D. Cornu, H. Vincent, J. Bouix, Adv. Func. Mater. 12 (2002) 228.
[33] S. Bernard, F. Chassagneux, M.P. Berthet, H. Vincent, J. Bouix, J. Eur. Ceram. Soc. 22 (2002) 2047.
[34] S. Bernard, D. Cornu, P. Miele, H. Vincent, J. Bouix, J. Organometal. Chem. 657 (2002) 91.
[35] G. Mignani, C. Richard, R. Trichon, French Patent 2695645 (1992).
[36] R.S. Pease, Acta. Crystallogr. 5 (1952) 356.
[37] S. Alkoy, C. Toy, T. Gönül, A. Tekin, J. Eur. Ceram. Soc. 17 (1997) 1415.
[38] S.N. Patankar, J. Mater. Sci. Lett. 10 (1991) 1176.
[39] M. Hubacek, M. Ueki, T. Sato, V. Brozek, Thermochim. Acta 282/283 (1996) 359.
[40] J. Thomas, N.E. Weston, T.E. O'Connor, J. Am. Chem. Soc. 84 (1962) 4619.